Title

Soft X-ray Spectroscopy of a Complex Heterojunction in High-Efficiency Thin-Film Photovoltaics: Intermixing and Zn Speciation at the Zn(O,S)/Cu(In,Ga)Se2 Interface

Journal

ACS Applied Materials & Interfaces, 8(48)

ISSN

1944-8244

Authors

Mezher, Michelle

Garris, Rebekah

Mansfield, Lorelle M

et al.

Publication Date

2016-12-07

DOI

10.1021/acsami.6b09245

Peer reviewed

ACS APPLIED MATERIALS & INTERFACES

Research Article

www.acsami.org

Soft X-ray Spectroscopy of a Complex Heterojunction in High-Efficiency Thin-Film Photovoltaics: Intermixing and Zn Speciation at the Zn(O,S)/Cu(In,Ga)Se_2 Interface

Michelle Mezher,[*,†] Rebekah Garris,[‡] Lorelle M. Mansfield,[‡] Monika Blum,[†] Dirk Hauschild,[§,∥] Kimberly Horsley,[†] Douglas A. Duncan,[†] Wanli Yang,[⊥] Marcus Bär,[†,#,∇] Lothar Weinhardt,[†,§,∥] Kannan Ramanathan,[‡] and Clemens Heske[*,†,§,∥]

[†]Department of Chemistry and Biochemistry, University of Nevada, Las Vegas (UNLV), Las Vegas, Nevada 89154-4003, United States

[‡]National Renewable Energy Laboratory (NREL), Golden, Colorado 80401, United States

[§]Institute for Photon Science and Synchrotron Radiation (IPS), Karlsruhe Institute of Technology (KIT), 76344 Eggenstein-Leopoldshafen, Germany

[∥]Institute for Chemical Technology and Polymer Chemistry (ITCP), Karlsruhe Institute of Technology (KIT), 76128 Karlsruhe, Germany

[⊥]Advanced Light Source, Lawrence Berkeley National Laboratory, Berkeley, California 94720, United States

[#]Renewable Energy, Helmholtz-Zentrum Berlin für Materialien und Energie GmbH, 14109 Berlin, Germany

[∇]Institut für Physik und Chemie, Brandenburgische Technische Universität Cottbus-Senftenberg, 03046 Cottbus, Germany

ABSTRACT: The chemical structure of the Zn(O,S)/Cu(In,Ga)Se_2 interface in high-efficiency photovoltaic devices is investigated using X-ray photoelectron and Auger electron spectroscopy, as well as soft X-ray emission spectroscopy. We find that the Ga/(Ga+In) ratio at the absorber surface does not change with the formation of the Zn(O,S)/Cu(In,Ga)Se_2 interface. Furthermore, we find evidence for Zn in multiple bonding environments, including ZnS, ZnO, $Zn(OH)_2$, and ZnSe. We also observe dehydrogenation of the Zn(O,S) buffer layer after Ar^+ ion treatment. Similar to high-efficiency CdS/Cu(In,Ga)Se_2 devices, intermixing occurs at the interface, with diffusion of Se into the buffer, and the formation of S—In and/or S—Ga bonds at or close to the interface.

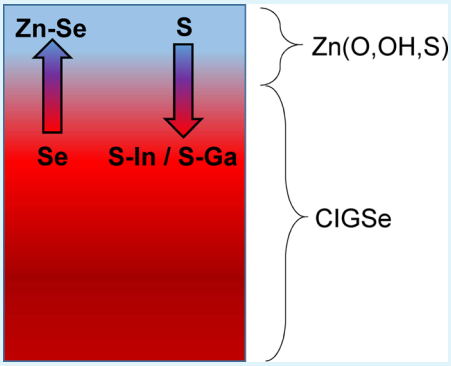

KEYWORDS: *chalcopyrite thin-film solar cell, chemical structure, alternative buffer layers, Zn(O,S), X-ray photoelectron spectroscopy, X-ray emission spectroscopy*

INTRODUCTION

Cu(In,Ga)Se_2 (CIGSe) thin-film photovoltaic devices have recently achieved a world-record efficiency of 22.6% on a laboratory scale utilizing a CdS buffer layer.[1] While *CdS*-based CIGSe devices have traditionally dominated the record efficiencies for this materials class,[2] other groups also report high conversion efficiencies (up to 22.0%) utilizing an alternative buffer layer based on Zn(O,S)[3−8] An understanding of the interface formation is crucial for optimizing these buffer layers and the buffer/absorber interface. While several studies have been published showing theoretically and experimentally derived interfacial band alignments,[9−14] there is a need to better understand the chemical interactions at the buffer/absorber interface, as this information can aid in deliberately tailoring the electronic band alignment. We note that current state-of-the-art Zn(O,S)-based devices feature a flat conduction band alignment.[14]

Previous studies have revealed a S/Se intermixing at the CdS/CIG(S)Se interface of high-efficiency thin-film devices with a chemical bath-deposited buffer layer.[15−18] Only few studies report on intermixing at the heterojunction between Zn(O,S) and chalcopyrites.[19,20] To gain better insights into the formation of the Zn(O,S)/CIGSe buffer layer and the chemical interactions at the interface in current state-of-the-art devices, we employ X-ray photoelectron spectroscopy (XPS), X-ray-excited Auger electron spectroscopy (XAES), and synchrotron-based soft X-ray emission spectroscopy (XES) on Zn(O,S)/CIGSe samples with varying buffer layer thickness.

Received: July 26, 2016
Accepted: November 11, 2016
Published: November 11, 2016

DOI: 10.1021/acsami.6b09245
ACS Appl. Mater. Interfaces 2016, 8, 33256−33263

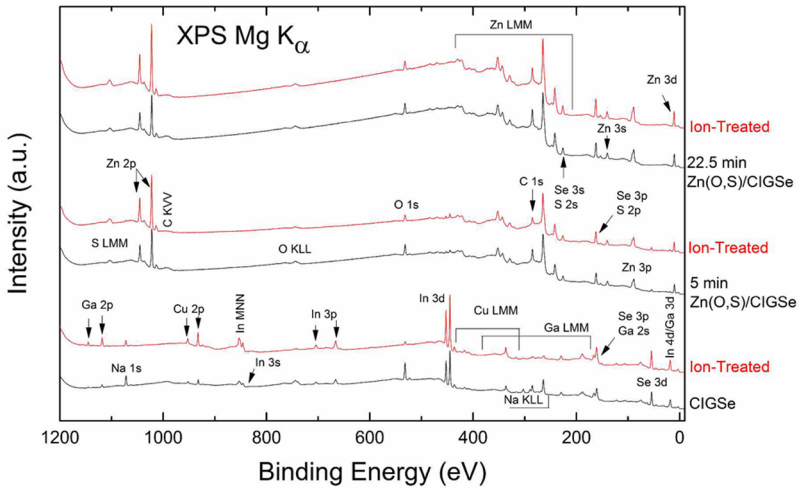

Figure 1. XPS survey spectra of the untreated (black) and 50 eV Ar^+-ion-treated (red) Zn(O,S)/CIGSe sample series: CIGSe bare absorber (bottom), 5 min Zn(O,S) (center), and 22.5 min Zn(O,S) (top).

EXPERIMENTAL SECTION

A full description of the samples can be found in ref 14. The sample set consists of a CIGSe three-stage bare absorber (nominal Ga/(Ga +In) ratio of 0.3) and three Zn(O,S)/CIGSe interface samples produced with varying Zn(O,S) chemical bath deposition (CBD) times (5, 10, and 22.5 min).[21,22]

XPS and XAES were conducted at UNLV, while XES was performed at the Advanced Light Source (ALS), Lawrence Berkeley National Laboratory. XPS measurements were taken with a SPECS PHOIBOS 150 MCD electron analyzer using Mg and Al K_α radiation and calibrated according to ref 23. The XES spectra were taken with the SALSA endstation[24] on beamline 8.0.1 at the ALS, utilizing a variable line-space grating (VLS) spectrometer. The spectra were calibrated using the prominent emission features of CdS.[25] The base pressure for the XPS and XES measurements was below 5×10^{-10} and 1×10^{-9} mbar, respectively.

The samples were briefly air-exposed (less than 5 min) at NREL before being packaged in a vacuum-sealed container. At UNLV, the samples were immediately introduced into an inert gas-filled glovebox, mounted on a sample holder, and transferred into the ultrahigh vacuum system. The samples were measured "as-received" and also after a low-energy (50 eV) Ar^+ ion treatment (two subsequent 60 min treatments for CIGSe, and three subsequent 20 min treatments for each of the 5 and 22.5 min Zn(O,S)/CIGSe samples) at low incidence angle.[26,27] XPS peaks were analyzed by fitting with Voigt functions, fixed spin−orbit splitting, coupled Gaussian and Lorentzian widths, and a linear background.[28] For quantification, inelastic mean free paths (IMFPs) were determined by the QUASES software.[29]

RESULTS AND DISCUSSION

XPS survey spectra of the bare CIGSe absorber and the 5 and 22.5 min Zn(O,S)/CIGSe samples are shown in Figure 1. The respective "as-received" spectra are shown in black, while the "ion-treated" spectra are shown in red. The pertinent CIGSe and Zn(O,S) photoemission and Auger lines (of Cu, In, Ga, Se, Zn, O, and S), as well as the Na lines are labeled, in addition to the peak associated with C. For the as-received CIGSe absorber, the O 1s peak is particularly pronounced, especially when the photoionization cross section is taken into account.[30,31] Due to the presence of this adsorbate layer, all high-binding (i.e., low-kinetic) energy peaks in the survey spectrum (e.g., Ga 2p, Cu 2p, In MNN, and Zn 2p) are suppressed in intensity. The low-energy ion treatment removes the majority of the adsorbate species, as well as most of the Na surface species, and thus the surface-sensitive high-binding energy peaks gain in intensity. In Figure 1 and the subsequent analysis, data after the first 20 min treatment is shown/used in order to minimize ion beam influences. In fact, as will be discussed later, the two subsequent ion treatments of the Zn(O,S)/CIGSe samples induced signs of surface alteration (dehydrogenation of the buffer). This indicates that Zn(O,S)—or more precisely the buffer hydroxide component (see below)—is more susceptible to changes due to low-energy ion treatments (and other irradiation) than the CIGSe absorber, CdS, or ZnO.[26,27,32,33] As the Zn(O,S) thickness is increased, Figure 1 shows that all peaks from the CIGSe absorber surface are attenuated, as expected. Small CIGSe-related core-level peaks are detected in the spectra of the thin Zn(O,S)/CIGSe sample (e.g., the In 3d and Se 3d peaks in Figure 1, center). In contrast, the 22.5 min Zn(O,S) sample shows no evidence of absorber-related peaks, suggesting that it is a continuous layer.

The Na peak intensity for the CIGSe bare absorber decreases with ion treatment, in parallel to a reduction of the oxygen and carbon signals [we note that the carbon signal for the Zn(O,S) layers is quite sizable, which we assign to an incorporation during the CBD process].[20] To gain further insight into the chemical state of Na on the CIGSe surface and the cause of this intensity decrease, the modified Auger parameters α' of Na were calculated. Figure 2 shows the Wagner plot[34] for the CIGSe absorber surface (red, ion-treatment times as indicated), along with relevant references (black).[35] The modified Auger parameter of α'_{Na} of sodium is calculated by summing the binding energy of the Na 1s core level and the kinetic energy of the $KL_{2,3}L_{2,3}$ Auger peak, and information about the chemical state is gained by comparing with reference data[34] along three axes: the Na 1s binding energy (abscissa), the Na KLL kinetic energy (ordinate), and α' (diagonal and right ordinate). The location of the CIGSe data on the Wagner plot is indicative of Na in an oxidized chemical environment. It is clearly different from metallic Na, but close to a large variety of O and/or C containing Na compounds [for example, we find evidence for a carbon species at ~289.7 eV, which would be in agreement with the presence of a (sodium) carbonate]. Thus, upon ion treatment, Na is likely to be desorbed along with the surface adsorbates. Based on earlier studies,[36−39] this is not unexpected for air-exposed CIGSe surfaces and is also assumed to happen in the chemical bath solution.

DOI: 10.1021/acsami.6b09245
ACS Appl. Mater. Interfaces 2016, 8, 33256−33263

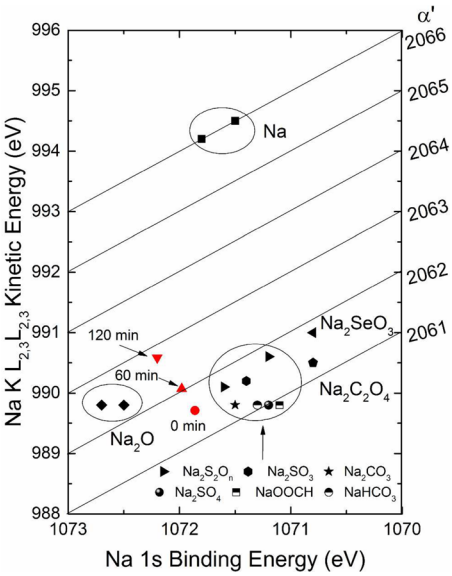

Figure 2. Modified Auger Parameter plot of Na 1s is shown before (red dot) and after different 50 eV Ar^+-ion energy treatment steps (red triangles) in comparison to references[33] in black (error bars are ±0.05 eV on both axes).

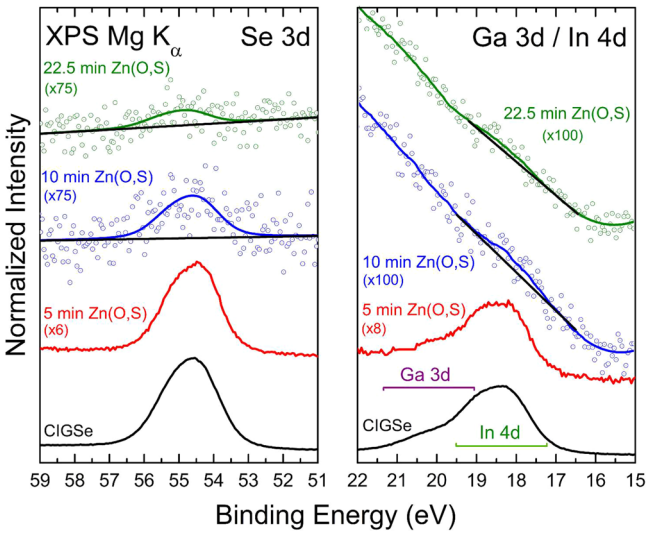

Figure 3. Mg K_α XPS spectra of the Se 3d peak (left) and the Ga 3d/In 4d region (right) for the CIGSe bare absorber and Zn(O,S)/CIGSe samples of varying thickness. To describe the 10 and 22.5 min spectra, the result of a fit with the CIGSe line shape and a linear background is shown. Multiplication factors are shown in parentheses.

Core-level peaks from the CIGSe absorber can be detected in the spectra of the thin Zn(O,S)/CIGSe sample, indicating that the 5 min CBD of Zn(O,S) results in a layer that is inhomogeneous and/or thinner than the region from which XPS information can be derived (note that XPS signals are governed by an exponential attenuation function, not a "box" function associated with a specific information depth). The absorber peaks detected for Cu, In, and Ga are of low intensity, while, in comparison, the Se 3d peak is larger, indicating the possibility of Se diffusion into the Zn(O,S) layer, as will be discussed now.

For the purpose of studying Se diffusion at the interface between Zn(O,S) and CIGSe, we also include the Zn(O,S)/CIGSe sample of intermediate thickness (10 min CBD). Figure 3 shows XPS spectra of the Se 3d peak (left) and the Ga 3d/In 4d peak (right) for the CIGSe bare absorber and the Zn(O,S)/CIGSe samples of increasing thickness. Due to their similar kinetic energies, the Se 3d, Ga 3d, and In 4d peaks are expected to have similar inelastic mean free paths (IMFPs), allowing the attenuation factors of these peaks to be compared as an initial step. The Se peak is strongly attenuated as the Zn(O,S) CBD time increases, but nevertheless it is still detectable even after the standard deposition time of 22.5 min. In contrast, the Ga 3d/and In 4d peaks of the 10 min Zn(O,S)/CIGSe and 22.5 min Zn(O,S)/CIGSe samples are extremely small (if present at all), even when magnified 100x (note that the Ga 3d/In 4d peaks lie on the onset of the O 2s peak, at ~26 eV, giving rise to the steep background observed for the 10 and 22.5 min sample). The detection of a Se signal even after 22.5 min of Zn(O,S) CBD suggests an outdiffusion of Se during the CBD process, similar to the CdS/CIGSe and CdS/CIGSSe interfaces.[15,17,18] All other absorber-related core-level and Auger peaks (not shown) were analyzed in a similar fashion, but no absorber-related peaks were visible for the 10 and 22.5 min Zn(O,S) CBD sample (note that these peaks are governed by shorter attenuation lengths due to their lower kinetic energy and will be discussed in greater detail below).

In order to analyze the possibility of Se, Ga, and/or In diffusion more quantitatively, Figure 4 presents an "effective

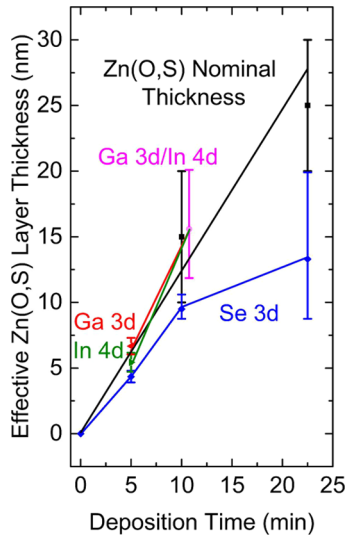

Figure 4. Effective Zn(O,S) layer thickness derived from Se 3d (blue), Ga 3d (red, 5 min), In 4d (green, 5 min), Ga 3d/In 4d combined (pink, 10 min), and nominal thickness (black) as a function of Zn(O,S) CBD time. The 10 min nominal thickness and Ga 3d/In 4d data were shifted slightly along the abscissa to differentiate between the data points.

Zn(O,S) layer thickness" as a function of the Zn(O,S) CBD time. The nominal thickness values (determined by Scanning Electron Microscopy images of corresponding cross sections at NREL) are shown as black data points and a best-fit line, while the effective thicknesses derived from the Se 3d, Ga 3d, and In 4d intensity attenuation are plotted in color and labeled (red, green, and pink colors: Ga 3d/In 4d, blue: Se 3d; solid lines connect the data points). If there is no diffusion of the element in question (in our case: Se), then the effective layer thickness should be similar to the nominal thickness, while it is expected

DOI: 10.1021/acsami.6b09245
ACS Appl. Mater. Interfaces 2016, 8, 33256−33263

to be below the nominal thickness line in the case of diffusion into the buffer layer. The effective thickness derived for a given peak is calculated using the following:

$$d_{\text{eff}} = \lambda \ln(I_0/I)$$

The IMFP is represented by λ, I_0 is the peak intensity in the bare absorber, and I is the peak intensity in the corresponding Zn(O,S)/CIGSe sample. We find that the Se 3d-based effective layer thickness lies significantly below the nominal thickness line, even when taking the error bars into account. Thus, the attenuation of the Se signal is lower than expected, suggesting that Se is diffusing into the buffer layer during the CBD process. In contrast, for the 5 min sample, the Ga 3d and In 4d effective thicknesses are larger and on (Ga) or very close (In) to the nominal line. For the 10 min sample, we note that the Ga 3d/In 4d region also includes the Mg K_β excitation of the O 2s line, which would give rise to a satellite approximately 9 eV[40] lower than the O 2s peak (~17 eV), and/or contributions from inelastically scattered Zn 3d electrons (peak at ~10 eV). Nevertheless, because the peak in the Ga 3d/In 4d region is clearly present for the 10 min sample, we show the effective layer thickness based on the attenuation of the combined Ga 3d/In 4d peak (pink), addressing the possible O 2s or Zn 3d area contributions by including a larger and asymmetric error bar. The effective layer thickness is again close to the nominal thickness line, suggesting that there is no significant diffusion of In or Ga into the buffer. For the 22.5 min sample, we argue that there is no detectable Ga 3d/In 4d peak, noting the absence of the (normally dominant) In $3d_{5/2}$ peak. The finding of Se outdiffusion into the Zn(O,S) buffer layer is reminiscent of the CdS/CIGSe interface, in which a pronounced S—Se exchange at the interface is found.[15,17,18] In the present case of a Zn(O,S) buffer, the diffusion of Se into the buffer layer leads us to speculate that in the proximity of the interface most likely Zn—Se bonds are formed.

Figure 5 shows fits of the Ga 3d/In 4d peaks of the bare CIGSe absorber and the 5 min Zn(O,S) sample in order to see if the Ga/(Ga+In) ratio at the absorber surface changes with the addition of the buffer layer. The peaks were fit with a linear background and Voigt profiles, using coupled Gaussian widths for all components, and coupled but separate Lorentzian widths for In and Ga, respectively. The ratios of the spin−orbit split peaks were fixed according to their multiplicity, along with their respective peak separation, 0.86 eV for In[41,42] and 0.46 eV for Ga.[43] The data points are shown with black dots, the In 4d components in green, the Ga 3d components in blue, and the resulting fit in red. The residual of the fit is shown below each spectrum (purple). We note that these shallow core levels already possess some band character, and thus the quality of the fit is surprisingly high, especially given all the above-mentioned boundary conditions included in the fit. The surface Ga/(Ga+In) ratio for the CIGSe absorber and 5 min Zn(O,S)/CIGSe samples are 0.33 and 0.32 (±0.10), respectively, indicating no change in the surface ratio with the addition of the buffer layer. Having thus gained a detailed description of the absorber surface, we can now take a closer look at the overlayer and its contributions to the interface formation.

As mentioned previously, the 5 and 22.5 min Zn(O,S)/CIGSe samples were ion treated in three 20 min increments. Figure 6(left) shows XPS spectra of the 22.5 min Zn(O,S)/CIGSe O 1s peak as a function of ion treatment time. Indeed, we see that with the first 20 min treatment, the O peak is reduced (partial removal of adsorbates) and the main peak

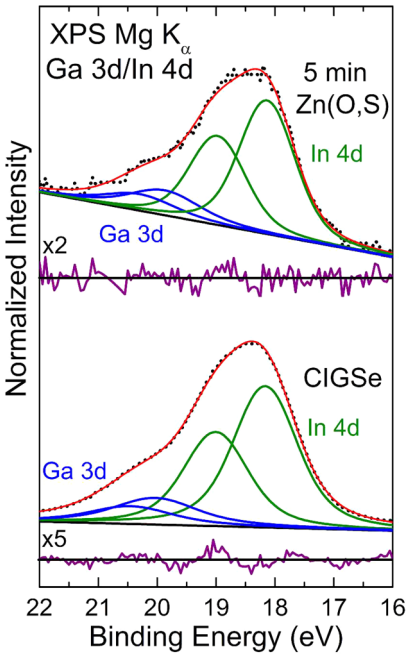

Figure 5. XPS detail spectra of the Ga 3d/In 4d region of the CIGSe absorber (bottom) and 5 min Zn(O,S) (top). Fit curves for In:Ga contributions to the peak are shown along with their respective residuals (purple).

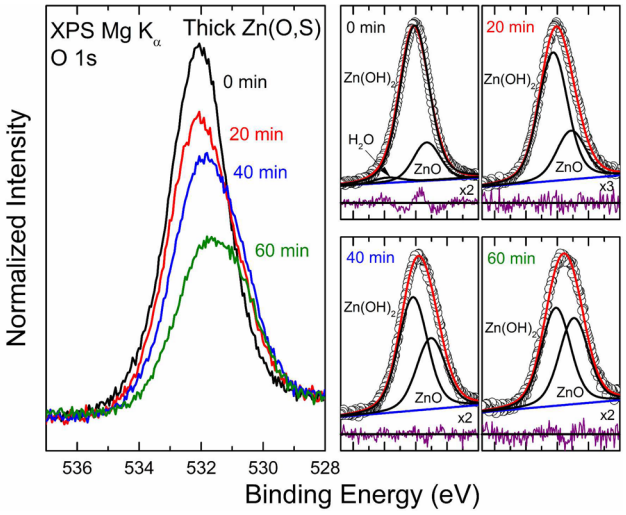

Figure 6. (Left) XPS spectra of the 22.5 min Zn(O,S) O 1s peak as a function of 50 eV Ar^+-ion treatment time. (Right) Fits of the O 1s peak show a change in OH/(OH+O) ratio as a function of ion treatment time.

position is identical to the untreated surface. However, with each subsequent treatment, the peak shifts toward lower BE and the shape changes as well. This is also true for the Zn and S peaks (not shown): the untreated and 20 min treated surface peak positions are identical, and with each subsequent treatment, the peak shifts to lower BE. The broadness and shape of the O 1s peak suggest that there are multiple chemical species of O in the (untreated) Zn(O,S) film. On the right of Figure 6, a fit analysis of the peak (as a function of ion treatment) shows that at least three species are present at the untreated surface, and at least two O species after each treatment. The peaks were normalized to peak height in order

DOI: 10.1021/acsami.6b09245
ACS Appl. Mater. Interfaces 2016, 8, 33256−33263

to easily visualize changes in peak component ratios. The peaks were fit with a linear background, identical Gaussian widths, identical Lorentzian widths, and fixed positions for all species. The residuals shown below the spectra indicate that the quality of the fit is quite high for the ion-treated surfaces. In contrast, the untreated O 1s peak shows a characteristic oscillation, which can be reduced by decoupling the Lorentzian width of this fit from that of the other three spectra. We thus derive that the spectrum of the untreated surface is a convolution of *at least* three species. Because there is a reduction in the O 1s peak intensity with the first ion treatment step, we believe that such additional species need to be ascribed to surface adsorbates. Based on their binding energies, the three components for the peak prior to ion treatment are assigned to H_2O, $Zn(OH)_2$, and ZnO.[35,44] For the peaks after ion treatment, the components are assigned to $Zn(OH)_2$ and ZnO only. The presence of $Zn(OH)_2$ suggests that the dehydrogenation of the Zn(O,S) layer during deposition is incomplete, indicating that a better description of this layer would be "Zn(O,OH,S)". Also, it cannot be ruled out that $Zn(OH)_2$ might be formed at the surface during the (brief) air exposure. The fits of the O 1s peaks show that, with increasing ion treatment time, the OH/(O+OH) ratio changes—a reduction in $Zn(OH)_2$ and an increase in ZnO suggests that the hydroxide component of the Zn(O,S) buffer surface is more susceptible to the low-energy Ar^+-ion treatment than, e.g., the ZnO surface commonly used as a window layer in CIGSe devices. This beam-induced dehydrogenation is not unexpected, as similar results have been found utilizing intense X-rays and electron flood gun irradiation on $Zn(OH)_2$-rich samples.[32,33] Nevertheless, we use data obtained after the first 20 min ion treatment for further analysis because this surface represents the best compromise between reduced contributions from surface adsorbates and minimal ion beam damage.

The Zn $2p_{3/2}$ and S 2p/Se 3p spectra for the 5 and 22.5 min Zn(O,S)/CIGSe samples are shown in Figure 7, along with the binding energy markers for several references.[35,44] Because the binding energies of the Zn references overlap (left), and because the observed peak is rather broad, it does not allow for an unambiguous assignment of the different species. This is not necessarily surprising—so far, our analysis has suggested three

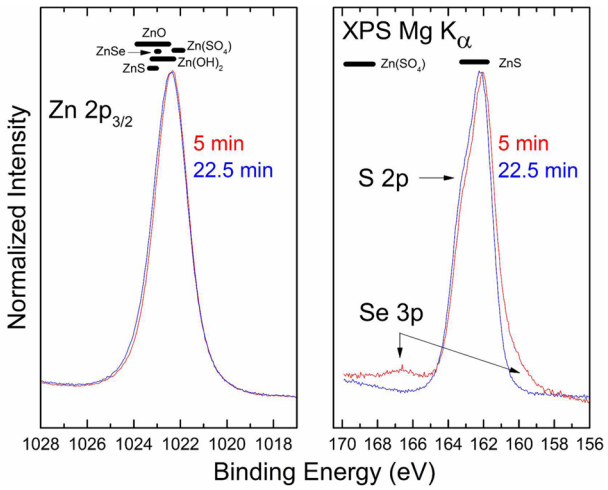

Figure 7. XPS spectra of the Zn $2p_{3/2}$ peak (left) and S 2p/Se 3p peaks (right) for the 5 and 22.5 min Zn(O,S) samples. Reference peak positions[33] are indicated above both peaks.

local bonding partners for Zn, namely O and OH from the O 1s peak fit and Se from the diffusion analysis. Furthermore, bonding to sulfur is also expected for the Zn(O,S) film surfaces. The S 2p/Se 3p spectra (right) show (a) the presence of sulfur in a sulfide environment, as expected, (b) the presence of Se for the 5 min samples (as discussed above; note that the Se 3p peak is much weaker than the Se 3d peak, and hence it is not seen for the 22.5 min sample), and (c) no evidence for sulfates on the surface.

XES spectra of the S $L_{2,3}$ and Se $M_{2,3}$ emission as a function of Zn(O,S) CBD time, excited nonresonantly with a photon energy of 180 eV, are presented in Figure 8. The CIGSe

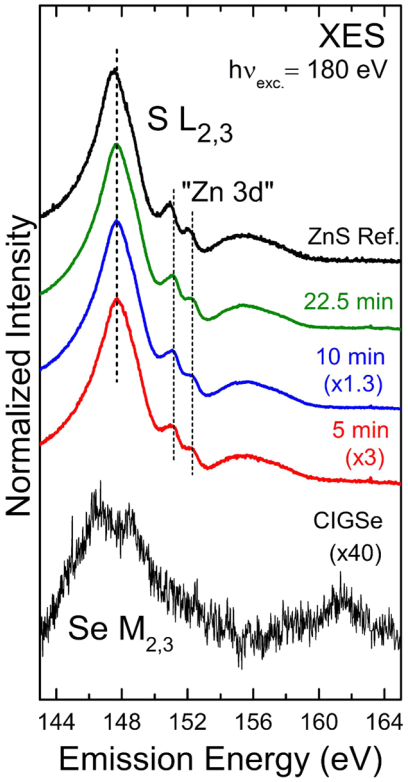

Figure 8. S $L_{2,3}$ and Se $M_{2,3}$ emission of the Zn(O,S)/CIGSe interface as a function of CBD time and a ZnS reference. Multiplication factors are shown in parentheses.

spectrum shows the Se $M_{2,3}$ emission, while the Zn(O,S)/CIGSe samples are dominated by S $L_{2,3}$ emission. The magnification factors at the right-hand side of each spectrum show that the Se $M_{2,3}$ is significantly weaker than the S $L_{2,3}$ emission. The intensity differences between the Se $M_{2,3}$ and S $L_{2,3}$ emission are due to the difference in fluorescence yield for the S 3s to S 2p transition (S $L_{2,3}$) and the Se 4s to Se 3p transition (Se $M_{2,3}$). As the Zn(O,S) layer is deposited, the characteristic spectrum of ZnS emerges. In particular, the two features at ~151.2 and ~152.4 eV (in the ZnS reference) are associated with electrons from the Zn 3d-derived band decaying into the S $2p_{1/2}$ and S $2p_{3/2}$ core holes. We do note that the Zn 3d-derived features are slightly shifted toward lower emission energies (by ~0.2 eV), indicating a different Zn chemical environment due to the presence of multiple Zn species (ZnS, ZnSe, $Zn(OH)_2$, and ZnO). There is no evidence of sulfates, as seen by the lack of a dominant peak at ~161 eV,[32,45] in contrast to a photoinduced sulfate formation observed for ILGAR-Zn(O,OH)/CIGSSe samples.[32,45]

DOI: 10.1021/acsami.6b09245
ACS Appl. Mater. Interfaces 2016, 8, 33256−33263

To gain insights into the component(s) contributing to the 5 and 10 min spectra, the 22.5 min spectrum [i.e., the S $L_{2,3}$ emission of the Zn(O,S) overlayer] was subtracted after normalizing all spectra to overall peak area. The resulting difference spectra are presented in Figure 9 a). The 5 min

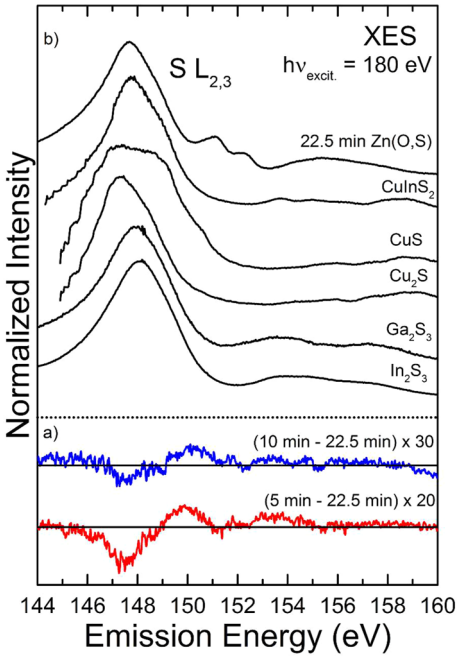

Figure 9. (a) Difference spectra from subtracting the 22.5 min Zn(O,S) S $L_{2,3}$ emission from the 5 min (red) and 10 min (blue) spectra. (b) 22.5 min Zn(O,S) spectrum and reference spectra for comparison.

difference (red) and the 10 min difference (blue) both show a dip at ~147.5 eV and a maximum at 150 eV, which we interpret as a spectral-weight shift of the main S $L_{2,3}$ peak. Comparison with reference compounds (Ga_2S_3, In_2S_3, $CuInS_2$, CuS, and Cu_2S) and the original 22.5 min Zn(O,S) spectrum [Figure 9 b)] suggests that this could be indicative of a different chemical environment of the sulfur atoms near the interface. Furthermore, we observe a maximum at ~153.5 eV which is most intense for the 5 min Zn(O,S) sample; at this energy, Ga_2S_3, In_2S_3, and $CuInS_2$ all exhibit additional partial density of states. A strong contribution of S—Cu bonds can, however, likely be ruled out due to the absence of any spectral difference at ~159 eV (i.e., the region of the Cu 3d contributions in $CuInS_2$ and the Cu sulfides). The difference spectra thus suggest that, in addition to the S—Zn bonding environment in the Zn(O,S) buffer layer, additional S chemical bonding environments are present at the interface to the CIGSe absorber, most likely in an S—In and/or S—Ga bonding environment, similar to what has been previously observed for the CdS/CIGSe interface.

CONCLUSIONS

The Zn(O,S)/CIGSe interface has been investigated using XPS, XAES, and XES to investigate the chemical structure. Detailed analysis of the bare CIGSe absorber and Zn(O,S)/CIGSe samples of varying CBD times allowed for a comprehensive analysis of the chemical interactions at this interface. We find evidence for an upward diffusion of Se into the buffer layer, most likely in a Zn—Se environment, and intermixing of S at the interface, most likely in an S—In and/or S—Ga environment. We find multiple chemical environments of Zn, best described by (a mixture of) ZnO, $Zn(OH)_2$, ZnS, and ZnSe. There is no evidence for sulfates in the Zn(O,S) layer (photoinduced or otherwise), but we do find evidence for Ar^+ ion beam-induced dehydrogenation of the Zn(O,S) layer. The resulting chemical interactions during the Zn(O,S)/CIGSe interface formation are found to be similar to those at the CdS/CIGSe interface,[15,17,18] but feature a higher degree of complexity with respect to the local chemical environment of the group II component.

AUTHOR INFORMATION

Corresponding Authors

*Phone: (702) 895-5078. Fax: (702) 895-4072. E-mail: mezherm@unlv.nevada.edu (M.M.).

*Phone: (702) 895-2694. Fax: (702) 895-4072. E-mail: heske@unlv.nevada.edu (C.H.).

ORCID

Michelle Mezher: 0000-0002-2663-6803

Dirk Hauschild: 0000-0001-9088-8944

Notes

The authors declare no competing financial interest.

ACKNOWLEDGMENTS

We gratefully acknowledge funding from the Department of Energy (DOE) through the F-PACE Partnership (NREL subcontract No. ZEJ-2-22082-0.1). M. Bär acknowledges funding by the Impuls- und Vernetzungsfonds of the Helmholtz Association (VH-NG-423). The Advanced Light Source is supported by the Director, Office of Science, Office of Basic Energy Sciences, of the U.S. Department of Energy under Contract No. DE-AC02-05CH11231.

REFERENCES

(1) Jackson, P.; Wuerz, R.; Hariskos, D.; Lotter, E.; Witte, W.; Powalla, M. Effects of Heavy Alkali Elements in Cu(In,Ga)Se_2 Solar Cells with Efficiencies up to 22.6%. *Phys. Status Solidi RRL* **2016**, *10* (8), 583−586.

(2) Green, M. A.; Emery, K.; Hishikawa, Y.; Warta, W.; Dunlop, E. D. Solar Cell Efficiency Tables (version 48). *Prog. Photovoltaics* **2016**, *24* (1), 905−913.

(3) Nakamura, M.; Yoneyama, N.; Horiguchi, K.; Iwata, Y.; Yamaguchi, K.; Sugimoto, H.; Kato, T. Recent R&D Progress in Solar Frontier's Small-sized Cu(In,Ga) (SeS)2 Solar Cells. *IEEE Photovoltaic Spec. Conf., 40th* **2014**, 0107−0110.

(4) Friedlmeier, T. M.; Jackson, P.; Bauer, A.; Hariskos, D.; Kiowski, O.; Wuerz, R.; Powalla, M. Improved Photocurrent in Cu(In,Ga)Se_2 Solar Cells: From 20.8% to 21.7% Efficiency with CdS Buffer and 21.0% Cd-Free. *IEEE J. Photovolt.* **2015**, *5* (5), 1487−1491.

(5) Contreras, M. A.; Nakada, T.; Hongo, M.; Pudov, A. O.; Sites, J. R. ZnO/ZnS(O,OH)/Cu(In,Ga)Se_2/Mo Solar Cell with 18.6% Efficiency. *Proceedings of 3rd World Conference on Photovoltaic Energy Conversion* **2003**, *1*, 570−573.

(6) Hariskos, D.; Menner, R.; Jackson, P.; Paetel, S.; Witte, W.; Wischmann, W.; Powalla, M.; Bürkert, L.; Kolb, T.; Oertel, M.; Dimmler, B.; Fuchs, B. New Reaction Kinetics for a High-Rate Chemical Bath Deposition of the Zn(S,O) Buffer Layer for Cu(In,Ga)Se_2-Based Solar Cells. *Prog. Photovoltaics* **2012**, *20* (5), 534−542.

(7) Klenk, R.; Steigert, A.; Rissom, T.; Greiner, D.; Kaufmann, C. A.; Unold, T.; Lux-Steiner, M. C. Junction Formation by Zn(O,S) Sputtering Yields CIGSe-Based Cells with Efficiencies Exceeding 18%. *Prog. Photovoltaics* **2014**, *22* (2), 161−165.

DOI: 10.1021/acsami.6b09245
ACS Appl. Mater. Interfaces 2016, 8, 33256−33263

(8) Takuya, K. Atsugi Research Center, Solar Frontier K.K., presentation at the 7th International Workshop on CIGS Solar Cell Technology (IW-CIGSTech 7), 32nd EU PVSEC, June 23, 2016, Munich, Germany.
(9) Bär, M.; Ennaoui, A.; Klaer, J.; Sáez-Araoz, R.; Kropp, T.; Weinhardt, L.; Heske, C.; Schock, H.-W.; Fischer, C.-H.; Lux-Steiner, M. C. The Electronic Structure of the [Zn(S,O)/ZnS]/$CuInS_2$ Heterointerface − Impact of Post-Annealing. *Chem. Phys. Lett.* **2006**, *433* (1−3), 71−74.
(10) Grimm, A.; Just, J.; Kieven, D.; Lauermann, I.; Palm, J.; Neisser, A.; Rissom, T.; Klenk, R. Sputtered Zn(O,S) for Junction Formation in Chalcopyrite-Based Thin Film Solar Cells. *Phys. Status Solidi RRL* **2010**, *4* (5−6), 109−111.
(11) Kieven, D.; Grimm, A.; Lauermann, I.; Lux-Steiner, M. C.; Palm, J.; Niesen, T.; Klenk, R. Band Alignment at Sputtered ZnS_x O_{1-x}/Cu(In,Ga) $(Se,S)_2$ Heterojunctions. *Phys. Status Solidi RRL* **2012**, *6* (7), 294−296.
(12) Terada, N.; Widodo, R. T.; Itoh, K.; Kong, S. H.; Kashiwabara, H.; Okuda, T.; Obara, K.; Niki, S.; Sakurai, K.; Yamada, A.; Ishizuka, S. Characterization of Interface Nature and Band Alignment in CBD-CdS/Cu(In,Ga)Se_2 Bi-Layer Structure by Photoemission and Inverse Photoemission Spectroscopy. *Thin Solid Films* **2005**, *480−481*, 183−187.
(13) Platzer-Björkman, C.; Törndahl, T.; Abou-Ras, D.; Malmström, J.; Kessler, J.; Stolt, L. Zn(O,S) Buffer Layers by Atomic Layer Deposition in Cu(In,Ga)Se_2 Based Thin Film Solar Cells: Band Alignment and Sulfur Gradient. *J. Appl. Phys.* **2006**, *100* (4), 044506−9.
(14) Mezher, M.; Garris, R.; Mansfield, L. M.; Horsley, K.; Blum, M.; Duncan, D. A.; Weinhardt, L.; Rosenberg, S.; Bar, M.; Ramanathan, K.; Heske, C. Electronic Structure of the Zn(O,S)/Cu(In,Ga)Se_2 Thin-Film Solar Cell Interface. *Prog. Photovoltaics* **2016**, *24* (8), 1142−1148.
(15) Heske, C.; Eich, D.; Fink, R.; Umbach, E.; van Buuren, T.; Bostedt, C.; Terminello, L. J.; Kakar, S.; Grush, M. M.; Callcott, T. A.; Himpsel, F. J.; Ederer, D. L.; Perera, R. C. C.; Riedl, W.; Karg, F. Observation of Intermixing at the Buried CdS/Cu(In, Ga)Se_2 Thin Film Solar Cell Heterojunction. *Appl. Phys. Lett.* **1999**, *74* (10), 1451−1453.
(16) Heske, C. Spectroscopic Investigation of Buried Interfaces and Liquids with Soft X-Rays. *Appl. Phys. A: Mater. Sci. Process.* **2004**, *78* (6), 829−835.
(17) Pookpanratana, S.; Repins, I.; Bär, M.; Weinhardt, L.; Zhang, Y.; Félix, R.; Blum, M.; Yang, W.; Heske, C. CdS/Cu(In,Ga)Se_2 Interface Formation in High-Efficiency Thin Film Solar Cells. *Appl. Phys. Lett.* **2010**, *97* (7), 074101.
(18) Weinhardt, L.; Bär, M.; Pookpanratana, S.; Morkel, M.; Niesen, T. P.; Karg, F.; Ramanathan, K.; Contreras, M. A.; Noufi, R.; Umbach, E.; Heske, C. Sulfur Gradient-Driven Se Diffusion at the CdS/CuIn$(S,Se)_2$ Solar Cell Interface. *Appl. Phys. Lett.* **2010**, *96* (18), 182102.
(19) Bär, M.; Ennaoui, A.; Klaer, J.; Kropp, T.; Sáez-Araoz, R.; Lehmann, S.; Grimm, A.; Lauermann, I.; Loreck, C.; Sokoll, S.; Schock, H.-W.; Fischer, C.-H.; Lux-Steiner, M. C.; Jung, C. Intermixing at the Heterointerface between ZnS/Zn(S,O) Bilayer Buffer and $CuInS_2$ Thin Film Solar Cell Absorber. *J. Appl. Phys.* **2006**, *100* (6), 064911.
(20) Eicke, A.; Ciba, T.; Hariskos, D.; Menner, R.; Tschamber, C.; Witte, W. Depth Profiling with SNMS and SIMS of Zn(O,S) Buffer Layers for Cu(In,Ga)Se_2 Thin-Film Solar Cells. *Surf. Interface Anal.* **2013**, *45* (13), 1811−1820.
(21) Ramanathan, K.; Mann, J.; Glynn, S.; Christensen, S.; Pankow, J.; Li, J.; Scharf, J.; Mansfield, L.; Contreras, M.; Noufi, R. A Comparative Study of Zn(O,S) Buffer Layers and CIGS Solar Cells Fabricated by CBD, ALD, and Sputtering. *IEEE Photovoltaic Spec. Conf., 38th* **2012**, 001677−001681.
(22) Contreras, M. A.; Egaas, B.; Ramanathan, K.; Hiltner, J.; Swartzlander, A.; Hasoon, F.; Noufi, R. Progress toward 20% Efficiency in Cu(In,Ga)Se_2 Polycrystalline Thin-Film Solar Cells. *Prog. Photovoltaics* **1999**, *7* (4), 311−316.
(23) Seah, M. P. Summary of ISO/TC 201 Standard: VII ISO 15472:2001-surface Chemical Analysis-x-Ray Photoelectron Spectrometers-calibration of Energy Scales. *Surf. Interface Anal.* **2001**, *31* (8), 721−723.
(24) Blum, M.; Weinhardt, L.; Fuchs, O.; Bär, M.; Zhang, Y.; Weigand, M.; Krause, S.; Pookpanratana, S.; Hofmann, T.; Yang, W.; Denlinger, J. D.; Umbach, E.; Heske, C. Solid and Liquid Spectroscopic Analysis (SALSA)–a Soft X-Ray Spectroscopy Endstation with a Novel Flow-through Liquid Cell. *Rev. Sci. Instrum.* **2009**, *80* (12), 123102.
(25) Weinhardt, L.; Fuchs, O.; Fleszar, A.; Bär, M.; Blum, M.; Weigand, M.; Denlinger, J. D.; Yang, W.; Hanke, W.; Umbach, E.; Heske, C. Resonant Inelastic Soft X-Ray Scattering of CdS: A Two-Dimensional Electronic Structure Map Approach. *Phys. Rev. B: Condens. Matter Mater. Phys.* **2009**, *79* (16), 165305.
(26) QUASES-IMFP-TPP2M program based on the following: Tanuma, S.; Powell, C. J.; Penn, D. R. Calculations of Electron Inelastic Mean Free Paths. V. Data for 14 Organic Compounds Over the 50−2000 eV range. *Surf. Interface Anal.* **1994**, *21*, 165−176.
(27) Weinhardt, L.; Heske, C.; Umbach, E.; Niesen, T. P.; Visbeck, S.; Karg, F. Band Alignment at the i-ZnO/CdS Interface in Cu(In,Ga)$(S,Se)_2$ Thin-Film Solar Cells. *Appl. Phys. Lett.* **2004**, *84* (16), 3175−3177.
(28) Morkel, M.; Weinhardt, L.; Lohmüller, B.; Heske, C.; Umbach, E.; Riedl, W.; Zweigart, S.; Karg, F. Flat Conduction-Band Alignment at the CdS/$CuInSe_2$ Thin-Film Solar-Cell Heterojunction. *Appl. Phys. Lett.* **2001**, *79* (27), 4482−4484.
(29) Wojdyr, M. Fityk: A General-Purpose Peak Fitting Program. *J. Appl. Crystallogr.* **2010**, *43* (5−1), 1126−1128.
(30) Scofield, J. H. Hartree-Slater Subshell Photoionization Cross-Sections at 1254 and 1487 eV. *J. Electron Spectrosc. Relat. Phenom.* **1976**, *8* (2), 129−137.
(31) Yeh, J. J.; Lindau, I. Atomic Subshell Photoionization Cross Sections and Asymmetry Parameters: $1 \leqslant Z \leqslant 103$. *At. Data Nucl. Data Tables* **1985**, *32* (1), 1−155.
(32) Reichardt, J.; Bär, M.; Grimm, A.; Kötschau, I.; Lauermann, I.; Sokoll, S.; Lux-Steiner, M. C.; Fischer, C.-H.; Heske, C.; Weinhardt, L.; Fuchs, O.; Jung, C.; Gudat, W.; Niesen, T. P.; Karg, F. Inducing and Monitoring Photoelectrochemical Reactions at Surfaces and Buried Interfaces in Cu(In,Ga)$(S,Se)_2$ Thin-Film Solar Cells. *Appl. Phys. Lett.* **2005**, *86* (17), 172102.
(33) Duchoslav, J.; Steinberger, R.; Arndt, M.; Stifter, D. XPS Study of Zinc Hydroxide as a Potential Corrosion Product of Zinc: Rapid X-Ray Induced Conversion into Zinc Oxide. *Corros. Sci.* **2014**, *82*, 356−361.
(34) Moretti, G. Auger Parameter and Wagner Plot in the Characterization of Chemical States by X-Ray Photoelectron Spectroscopy: A Review. *J. Electron Spectrosc. Relat. Phenom.* **1998**, *95* (2−3), 95−144.
(35) Moulder, J. F. *Handbook of X-Ray Photoelectron Spectroscopy: A Reference Book of Standard Spectra for Identification and Interpretation of XPS Data*; Physical Electronics Division, Perkin-Elmer Corporation, 1992.
(36) Heske, C.; Eich, D.; Groh, U.; Fink, R.; Umbach, E.; van Buuren, T.; Bostedt, C.; Franco, N.; Terminello, L.; Grush, M.; Callcott, T.; Himpsel, F.; Ederer, D.; Perera, R. C.; Riedl, W.; Karg, F. Self-Limitation of Na Content at the CdS/Cu(In,Ga)Se_2 Solar Cell Heterojunction. *Thin Solid Films* **2000**, *361−362*, 360−363.
(37) Heske, C.; Fink, R.; Umbach, E.; Riedl, W.; Karg, F. Na-induced Effects on the Electronic Structure and Composition of Cu(In,Ga)Se_2 Thin-film Surfaces. *Appl. Phys. Lett.* **1996**, *68* (24), 3431−3433.
(38) Heske, C.; Richter, G.; Chen, Z.; Fink, R.; Umbach, E.; Riedl, W.; Karg, F. Influence of Na and H_2O on the Surface Properties of Cu(In,Ga)Se_2 Thin Films. *J. Appl. Phys.* **1997**, *82* (5), 2411−2420.
(39) Heske, C.; Eich, D.; Fink, R.; Umbach, E.; Kakar, S.; van Buuren, T.; Bostedt, C.; Terminello, L. J.; Grush, M. M.; Callcott, T. A.; Himpsel, F. J.; Ederer, D. L.; Perera, R. C. C.; Riedl, W.; Karg, F. Localization of Na Impurities at the Buried CdS/Cu(In, Ga)Se_2 Heterojunction. *Appl. Phys. Lett.* **1999**, *75* (14), 2082−2084.

DOI: 10.1021/acsami.6b09245
ACS Appl. Mater. Interfaces 2016, 8, 33256−33263

(40) Klauber, C. *Appl. Surf. Sci.*, Vol. *70*−*71*, Part 1, 2 June **1993**, Pages 35−39.10.1016/0169-4332(93)90393-P
(41) Gebhardt, R. K.; Sloboshanin, S.; Schaefer, J. A.; Chassé, T. Arsenic Interlayers at the Sn/InP(001) Interface. *Appl. Surf. Sci.* **1999**, *142* (1−4), 94−98.
(42) Cherkashinin, G.; Krischok, S.; Himmerlich, M.; Ambacher, O.; Schaefer, J. A. Electronic Properties of C_{60} /InP(001) Heterostructures. *J. Phys.: Condens. Matter* **2006**, *18* (43), 9841.
(43) Beach, R. A.; Piquette, E. C.; McGill, T. C. XPS Study of Oxygen Adsorption on (3 × 3) Reconstructed MBE Grown GaN Surfaces. *MRS Online Proc. Libr.* **1998**, *537* (S1), Art. No. G6.26.10.1557/PROC-537-G6.26
(44) NIST X-ray Photoelectron Spectroscopy (XPS) Database Main Search Menu http://srdata.nist.gov/xps/main_search_menu.aspx (accessed Jan 13, 2016).
(45) Duncan, D. A.; Kephart, J. M.; Horsley, K.; Blum, M.; Mezher, M.; Weinhardt, L.; Häming, M.; Wilks, R. G.; Hofmann, T.; Yang, W.; Bär, M.; Sampath, W. S.; Heske, C. Characterization of Sulfur Bonding in CdS:O Buffer Layers for CdTe-Based Thin-Film Solar Cells. *ACS Appl. Mater. Interfaces* **2015**, *7* (30), 16382−16386.

DOI: 10.1021/acsami.6b09245
ACS Appl. Mater. Interfaces 2016, 8, 33256−33263